Shallow flank deformation at Cumbre Vieja volcano (Canary Islands): Implications on the stability of steep-sided volcano flanks at oceanic islands

Pablo J. González[1,*], Kristy F. Tiampo[2], Antonio G. Camacho[1] and José Fernández[1]

[1] Instituto de Astronomía y Geodesia (CSIC-UCM), Fac. Cc. Matemáticas, Plaza de Ciencias, 3, Ciudad Universitaria, 28045-Madrid, Spain

[2] Department of Earth Sciences, University of Western Ontario, Biological and Geological Sciences Building, London, ON, N6A 5B7, Canada

[*] Corresponding Author:

E-mail address: pjgonzal@mat.ucm.es

Full postal address:

Instituto de Astronomía y Geodesia (CSIC-UCM), Fac. Cc. Matemáticas,

Plaza de Ciencias, 3, Ciudad Universitaria, 28045-Madrid, Spain

Telephone: +34 913944634

Fax: +34 913944615

Submitted to *Earth and Planetary Science Letters* 13 January 2010

Reviewed 2 April 2010

Revised 19 May 2010

Accepted 24 June 2010

Abstract

Volcano flank instability has been recognized at many volcanoes around the globe. Structural, morphological, geodetic and geophysical evidence supports the continuous deformation of their flanks. While identification of instability has been recognized in well-documented examples, until recently the initial stages of such processes have been difficult to capture. Using a combination of geological, geodetic and geophysical data analysis, we study the stability of the Cumbre Vieja. New descending radar interferometric data, covering a volcanologically quiet period between 1992-2008 at Cumbre Vieja, indicate movement away from the satellite on the western volcano flank. Using an inversion of stacked velocity maps, we determine the geometry and slip for a near-horizontal dislocation beneath the western flank of Cumbre Vieja. Our ground deformation modelling results (position and depth) are in agreement with a low-density anomaly constrained by gravity data. The previously undetected intereruptive ground deformation at Cumbre Vieja volcano flanks was explained as an indicator of a kinematic passive response model of the flank, where the flanks were mobilized only during periods of magmatic activity (shallow dike intrusions) and remained stable and undeformed during intereruptive periods. Here, we present new results indicating that active creeping stress release due to gravitational loading is also a dominant deformation mechanism for (current) intereruptive periods at Cumbre Vieja, which would contribute positively to the stabilization of the edifice and reduce the associated hazard related to the volcano flank dynamics. This study at Cumbre Vieja can be considered as a prototype for similar volcanoes around the Macaronesian islands group (e.g. Fogo, Teide, El Hierro, Pico) and elsewhere.

Keywords: Volcano flank dynamics, Slope stability, Volcano geodesy, Canary Islands, La Palma, Radar Interferometry (InSAR)

1. Introduction

Volcanic edifices are some of the most rapidly growing geological structures on Earth. As a consequence, their flanks often tend to be deformed under structural instability. Since the occurrence of the 1980 Mt. St. Helens debris avalanche, volcano flank instability has been a subject of intensive research and monitoring (Lipman et al., 1981; Duffield et al., 1982; Clague and Denlinger, 1994; Moore et al., 1989, 1994; Holcomb and Searle, 1991; Masson 1996; Day et al., 1999a and 1999b; McGuire, 1996; 2006). A list of mechanisms producing mass-wasting processes includes, but is not limited to, spreading and/or slumping, basal décollements, landslides and flank failures. In particular, at ocean-island volcanoes, the risk associated with such processes is, in part, due to its likely tsunamigenic potential and often the flank deformation is used as indicator of the likelihood of such a process (Cervelli et al., 2002; Ward, 2002; Cervelli, 2004). The identification of continuous and episodic aseismic slip at faults in volcanic regions has been identified geodetically at the mobile southern flank of Kilauea (Denlinger and Okubo, 1995; Owen et al., 1995, 2000; Cervelli et al., 2002) and the eastern flank of Mt. Etna (Froger et al., 2001). At both places, slow continuous and rapid sudden episodic transients have been recorded at basal and intravolcanic fault surfaces. Continuous aseismic slip has been quantified using classical geodetic techniques, as well as GPS surveys (Owen et al., 2000) and DInSAR data (Froger et al., 2001; Lundgren et al., 2003). At the moment, the ground motion due to episodic sliding

(Slow Slip Events, SSE) on these surfaces has been imaged using only continuous GPS (Cervelli et al., 2002; Brooks et al., 2006, 2008; Segall et al., 2006).

FIGURE 1

Using the rationale mentioned by Day et al. (1999a), two different types of unstable flanks can be distinguished at volcanoes, using the flank slopes as a parameter. Some gentle sloping (Kilauean-like) volcanoes are associated with high flank deformation dynamics (Fig. 1a). Conversely, steep-sided (Macaronesian-like) volcanoes are largely associated with minimal ground deformation (Fig. 1b). Both types of volcano flanks tend to stabilize through different mass-wasting processes (Holcomb and Searle, 1991; Morgan et al., 1994). Around the Canary Islands, as many as fourteen giant debris-avalanche deposits have been identified (Masson et al., 2002). Analysis of turbidite records in the Agadir basin 300 km north of the Canary Islands indicates that progressive and recurrent slumping flows correlate well with the occurrences of major debris avalanches on the Canary Islands (Wynn and Masson, 2003; Masson et al., 2006). This evidence raises the question as to whether such mass-wasting processes are sudden and occur with minimal precursory signals in heavy steep-sided volcano flanks, such as the Macaronesian volcanoes (Day et al., 1997; Day et al., 1999b). If the debris avalanches occurred as the consequence of many and multiple high-density flows, precursory signals such as progressive slumping and deformation might affect the unstable volcano flanks.

Interferometric Synthetic Aperture Radar (InSAR) can potentially help resolve slope stability questions. Continuous surface displacements related to progressive slumping

processes can be imaged with subcentimeter precision with InSAR and can be compared with the location of surface expressions and the inferred subsurface location of such processes. A link between the ground deformation and the inferred location of shallow active décollement would also suggest that aseismic slip and creep may be dominant or, at least, important mechanisms acting during the intereruptive periods of steep-sided volcanoes. Since modern space geodetic techniques were developed in the 1990's, neither a geodetic monitoring network nor an advanced satellite-based interferometric study has been carried out in such an environment, providing no constraints on the ongoing processes acting on such steep-sided volcanoes. The availability of more than 15 years of SAR images at Cumbre Vieja volcano could help to constrain the volcano flank deformation. In this paper, we combine radar interferometry with other observations to investigate the resulting surface displacements, and we discuss the implications for the stability of steep-sided volcanoes affected by aseismic slip and creeping.

2. Structure and Geology of La Palma

The island of La Palma is the second youngest of the Canarian Archipelago. It represents a salient example of steep-sided composite volcano. Its volcanic edifice rest upon the oceanic crust at a sea-floor depth of 4000 m., and the subaerial topographic elevations reach around 2500 m. The structural and geological development of La Palma is complex, with interactions between large intrusions linked with high effusive episodes inserted between erosional gap periods, together with gravitational mass-wasting phenomena (Carracedo et al., 2001). At least two debris avalanches have occurred at La Palma (Urgeles et al., 1999; Masson et al., 2002). Cumbre Vieja is the last volcanic expression of a succession of growing and overlapping volcanic centers in

La Palma. In the following two subsections we introduce the main characteristics of the La Palma structure and volcanology, which are relevant to the later discussion of the current structure and state of deformation.

FIGURE 2

2.1. Pre-Cumbre Vieja geological and structural evolution

La Palma Island began to grow onto the oceanic crust, probably > 4 Ma ago (Staudigel et al., 1986). Pre-Cumbre Vieja volcanic stratigraphy consisted of three fully overlapped shield volcanoes and a partly overlapping stratovolcano. The lower stratigraphic unit is called the basal complex (Staudigel et al., 1986) or seamount/submarine volcano series (Carracedo et al., 2001), a basic composition complex with a large amount of intrusives. The seamount series are outcropping at the base of the Caldera de Taburiente depression at a height of 1500 m., which indicates an uplift process either due to repetitive intrusions (Gallip et al., 2006) or of tectonic origin (Hildenbrand et al., 2003). Much of this deformation probably was accommodated under brittle conditions (Fernández et al., 2002a), also supported by the presence of low grade (~200-300 ºC) hydrothermal metasomatism rock alteration (de la Nuez, 1984). Currently, the submarine series clearly dips 50º to the SW (Fernández et al., 2002a).

The top of the SW tilted submarine series is marked by an erosive unconformity, overlaid by the *Taburiente I* or *Garafia* volcano stratigraphic unit, a buried basaltic shield volcano. Garafia volcano built rapidly from its central feeding system (1.72 – 1.20 Ma) and its activity abruptly ceased after the occurrence of a southward lateral collapse, which formed the so-called “Coebra” structure, a main subsurface

hydrogeological feature recognized at underground tunnels for groundwater abstraction (*galerías*) (Plan Hidrológico Insular de La Palma, 2001). This structure can be related to the "Playa de La Veta" debris avalanche submarine deposits (Urgeles et al., 1999).

Later, the magmatic activity migrated slightly southward, resulting in the *Taburiente II* or *Taburiente* volcano (1.08 – 0.44 Ma), fully overlapping the older Seamount and Garafia volcanoes. This unit is a thick unit with a central system and a triple armed rift zone structure (Carracedo et al., 2001). Progressively, the volcanic activity focused along the prominent topographic southern rift, the "Cumbre Nueva" ridge (0.77 – 0.56 Ma). Cumbre Nueva volume surpassed the lithostatic pressure at depths corresponding to the top of the tilted seamount series and/or the Playa de La Veta collapse scar, triggering a catastrophic collapse (0.5 Ma ago) forming Los Llanos de Aridane valley (Navarro and Coello, 1993; Ancoechea et al., 1994; Carracedo et al., 1998) and the submarine Cumbre Nueva debris avalanche deposits (Urgeles et al., 1999; Masson et al., 2002). Soon after, *Bejenado* stratovolcano started to fill the scar collapse (560 to 490 ka). Its magmatic activity showed declining production rates due to the diminished effect of unloading at the magma-source region (Guillou et al., 1998, 2001). Between Bejenado and the Northern shield volcanoes developed an erosive incision, the Caldera de Taburiente, which resulted in the thick *El Time* sedimentary unit (see, Fig. 2). Finally, the Cumbre Vieja volcano began to grow after activity finished at Bejenado.

2.2. Cumbre Vieja volcano-structural evolution

Currently, Cumbre Vieja volcano is the only active volcanic system on La Palma Island. Cumbre Vieja is a composite volcano of mafic lavas, with interbedded pyroclastics and sparse phonolitic domes, crystallized at shallow levels (Ancoachea et al., 1994; Day et

al., 1999a; Johansen et al., 2005). Topographically, it is a steep-sided volcano with 20-30º slopes that rises to almost 2 km above sea level. It has a subaerial area of 220 km^2 and an estimated volume of approximately 125 km^3 (Carracedo et al., 2001).

Several authors contributed to the Cumbre Vieja geological stratigraphy and its associated structural changes (Guillou et al., 1998; Carracedo et al. 1999; Day et al., 1999a; Guillou et al., 2001; Carracedo et al., 2001). In particular, we recommend a very detailed (1:25000) analysis of a geological and structural survey at Cumbre Vieja (Carracedo et al., 2001). To briefly summarize, Cumbre Vieja can be divided into three main periods and two clear stratigraphic units:

(1) The *Cliff-forming unit*, which is formed by the oldest dated rocks, indicating that Cumbre Vieja starts to grow 125 ka B.P. (Guillou et al., 1998), but probably before (Carracedo, 1999; Carracedo et al., 1999). From 125 to 80 ka, eruptive products focused on three distinct rift zones separated by roughly 120º, as shown in Fig. 3a (Guillou et al., 1998; Day et al., 1999a). The rift system was established with a high and distributed production rate throughout the three rifts (NW, NE and NS). Later, the production and growing rate decreased and the marine erosion became the dominant process (80-20 ka), also partly due to the relative low-stand sea level (Guillou et al., 1998; Carracedo, 1999).

(2) In the *platform-forming* unit (20 ka B.P.), the activity resumed, focusing along two of the three previous rift zones (NS and NE). In particular, the NE rift zone underwent high rates of eruptive activity. Contemporaneously, the magma focus migrated slightly northwards and, consequently, the NS rift-zone propagated to the north (Guillou et al.,

200 1998; 2001; Carracedo et al., 1999). It continued until 7 ka., when the NE activity
201 abruptly ceased. During that period (20-7 ka), apparently, the activity declined almost
202 entirely at the NW rift zone (Fig. 3b), probably due to an early manifestation of the
203 subsequent reorganization of the whole plumbing and shallow feeding system (Day et
204 al., 1999a).
205
206 (3) In the last 7 ka to present, a strong reorganization of the stress field of the shallow
207 plumbing system occurred as, *a)* eruptions along the NW and NE rifts stopped and
208 eruptive activity was concentrated on the axis of the NS rift zone that is prominent
209 today, and inside the western flank (Day et al., 1999a). *b)* At historical and subhistorical
210 times there have been seven eruptions, in ca. A.D. 1480, 1585, 1646, 1677, 1712, 1949,
211 and 1971 (Fig. 3c). During 1585, 1712 and partly during the 1949 eruptions along the
212 western flank, the eruptive vents opened in nearby E-W fissures reconfiguring the
213 pattern of fissural vents distribution (Day et al., 1999a). Most recently, *c)* an unusual
214 feature appeared during the 1949-summit eruption, a 4-meter downslip in a west-to-
215 southwest-facing normal fault (Day et al., 1999a; Klügel et al., 1999), see Fig. 3d-e.
216
217 Such structural evolution (new structural features) indicates a progressive increase of
218 the role of the NS rift as a preferentially magmatic path. Repeated, forceful shallow
219 intrusions along the NS rift zone tend to mobilize the western flank, which increases the
220 related hazards, as suggested by Day et al., (1999a).
221
222 **FIGURE 3**
223
224

3. Geodetic data analysis

3.1. Previous geodetic data

Previous geodetic studies that focused on the analysis of the stability of the western flank of Cumbre Vieja did not identify significant deformation rates using EDM, GPS and classical DInSAR (Moss et al., 1999; Massonnet and Sigmundsson, 2000; Fernández et al., 2002b). Recently, the ground deformation pattern at Cumbre Vieja volcano has been studied using a combination of geodetic techniques, a comparison of two temporal series of differential interferograms based on a single master approach (Perlock et al., 2008) and the analysis of a GPS network (Prieto et al., 2009). Although they reported significant ground deformation in the area of the last eruption, the Teneguia volcano, both studies lack evidence for conclusive and precise ground deformation (large estimated errors) on the western slopes of the Cumbre Vieja, partly due to an ERS SAR dataset that was limited in time and the sparse spatial coverage of the GPS network.

3.2. Interferometric data analysis

Studies of volcanic deformation have used SAR interferometry as a valuable resource for poorly monitored areas (Amelung et al., 2000; Anderssohn et al., 2009), as in the case of Cumbre Vieja volcano. Briefly, SAR interferometry records the phase delay caused between two temporally separated SAR images in the line-of-sight direction (pointing ~23º degrees from vertical, for ERS1/2 and I2-Envisat mode satellites) with subcentimetric precision for areas that remain coherent (ie. with stable ground reflectivity) during the observed period. The differential phase can be caused due to the topography, atmospheric perturbations and/or motion of the ground surface. If

topographic and atmospheric delays can be corrected or assumed negligible, InSAR can lead to precise ground deformation maps over large areas (Hanssen, 2001).

To better evaluate the expected current low rates of deformation at Cumbre Vieja volcano (Moss et al., 1999; Perlock et al., 2008), we have extended the SAR dataset to include ENVISAT data and analyzed 25 SAR images acquired by the European Remote Sensing (ERS1/2) satellites between May 1992 and September 2000 (Table S1) and 19 ASAR images acquired by the ENVISAT satellite from March 2003 to February 2008 (Table S2), archived by the European Space Agency (ESA). We selected descending SAR images, roughly regularly sampled over the period studied (1992-2008), to obtain a detailed image map of the ground deformation at Cumbre Vieja volcano. We note that a similar analysis using ascending data is not feasible due to severe foreshortening that would result from the steep slopes of the western flank of Cumbre Vieja. Moreover, only five ascending ERS1/2 SAR images are archived in the ESA catalogues. Topographic contribution in the interferograms was cancelled using a local precise Spanish Instituto Geografico Nacional Digital Elevation Model with 25-meter posting ground resolution. Interferograms were computed using DORIS v.4.02 software with DEM-assisted co-registration (Kampes et al., 2003).

3.2.1 The importance of the atmospheric path delays

Due to the low deformation rates, single differential interferograms do not show clear ground deformation patterns, except for those with long temporal baselines that exhibit a rough subsidence signal around the Teneguia volcano area (Perlock et al., 2008). Deformation can be partly obscured by atmospheric perturbations consisting of turbulent mixing and tropospheric stratification (Hanssen et al., 2001). Water vapour

274 turbulence also produces path delays, but these signals typically do not correlate at
275 distances longer than the thickness of the boundary layer, typically 1.5-2.5 km
276 (Williams et al., 1998; Hanssen, 2001). Although, in general, turbulent path delay
277 effects have been demonstrated to be temporally uncorrelated at lag times longer than 1
278 day (Hanssen, 1998), at oceanic islands with strong topography turbulent effects
279 potentially can be both spatially and temporally correlated, reaching largely several
280 centimetres in line-of-sight (Foster et al., 2006). On the contrary, path delays due to the
281 thermal-topographic dependence account for differences in the water vapour content
282 with height, which is common around volcanoes accompanied by steep topographies
283 (Delacourt et al., 1998).
284
285 For the Canary Islands, the latter effect has been analysed using MODIS spectral
286 imagery. In particular, the tropospheric stratification effect has been shown to be the
287 dominant process in the lower troposphere (Eff-Darwich et al., 2009; Eff-Darwich et al.,
288 *in preparation*). In addition, a very limited, but useful, GPS-based Zenith Tropospheric
289 Delay (ZTD) analysis, using standard weekly EUREF products, was carried out for the
290 only two available public continuous GPS stations in the Canary Islands area. The GPS
291 stations are located at different heights and their ZTD time series shows magnitude of
292 the annual fluctuations depending on the GPS station altitude, suggesting that height
293 dependent water vapour delay plays an important role in the microwave propagation
294 measurements for any combination of temporal separated SAR images (Fig. S2).
295
296 *3.2.2 Atmospheric effect mitigation and averaged ground deformation maps*
297 As detailed earlier, we can not consider the atmospheric contribution to be negligible.
298 To deal with the dominant vertical troposphere contribution, we perform, on an

299 interferogram-by-interferogram basis, a correction procedure consisting of the
300 estimation of the best-fitting linear model between differential interferometric phase and
301 the elevation of each coherent point (Cavalié et al., 2007; Doin et al., 2009). In our
302 particular case, the use of a linear model in conjunction with the local topography may
303 correct the differential phase for atmospheric contribution, but at the same time it likely
304 will mask those ground deformation signals correlated with topography, which should
305 not be neglected at a steep volcano centred on the vertical axis of its magma feeding
306 systems. So, this method will be inefficient to detect global inflation/deflation beneath
307 the rift system, which will reproduce the local topography.
308
309 To enhance the signal-to-noise ratio of differential interferograms with ground motion
310 signal, we have stacked the atmospherically-corrected interferograms for long-interval
311 (longer than a year) and short-baseline interferograms (less than 300 meters) to reduce
312 the uncorrelated noise (Wright et al., 2001, 2004; Fialko, 2006), including any pixel that
313 exhibits good coherence (average coherence threshold > 0.3). We exclude short-time
314 separated interferograms in order to increase the reduction due to large strain rates in
315 such interferograms from turbulent tropospheric effects (Fig 4b and 4d). Stacking
316 involves averaging multiple (independent) interferograms, theoretically reducing the
317 level of atmospheric noise by a factor of $1/\sqrt{N}$ when averaging N independent
318 interferograms (Sandwell and Price, 1998; Wright et al., 2001). To evaluate the level of
319 correlated noise on each interferogram, we have computed empirical covariance
320 functions in the northern part of the island, where we do not expect deformation (Fig. 4a
321 and 4c).
322
323 **FIGURE 4**

3.2.3. InSAR ground deformation results

The northern half of La Palma exhibits a higher degree of temporal decorrelation due to the dense subtropical vegetation. This area has been inactive for the past 1 Ma (see sec. 2.1), so it is unlikely to be suffering from significant ground deformation processes. Moreover, the persistent uplift of the northern shield volcano has been estimated at an average rate of ~0.4 mm/yr for the El Time sedimentary formation and ~0.6 mm/yr for the submarine complex (Hildenbrand et al., 2003). Such a slow rate of vertical movement is difficult to recover with DInSAR techniques. Although sub-millimetric precision has been claimed (Colesanti and Wasowski, 2006), cross-validation tests show much lower precision in the determination of average ground motion velocity of ~1 mm/yr (Casu et al., 2005). Because of this, we have concentrated our ground deformation analysis in the active rift zone of Cumbre Vieja.

FIGURE 5

Our measurements using average LOS velocity maps from the 1992-2000 (Fig 5a) and 2003-2008 (Fig 5b) periods reveal two clear subsidence signals which can be detected at the Teneguia volcano area and on the western slopes of the Cumbre Vieja volcano (Fig. 5). The detected deformations were calculated using the descending orbit pass, so it could be either subsidence, westward motion, or a combination of the two.

3.3. GPS and gravimetric data

Results from an EDM/GPS network set up in 1994, for three campaigns spanning 1994 to 1997, indicate that residual motions were not significant (Moss et al., 1999). This has

been interpreted as confirmation that the fault (Fig. 2 and 3d) has been inactive since the 1949-eruption (Ward and Day, 2001). However, the very limited spatial coverage and difficulties in the observation strategy of the whole flank network means that it is only valid to measure strain rates around and near the 1949-fault (Moss et al., 1999). Geodetic observations of the entire western flank should be carried out using GPS. In 2006, a GPS network of 26 stations was designed and installed to cover the entire La Palma Island (Fig. 2). In the design of the network, a few previous precise GPS station coordinates (from 1994) computed for reference frame realizations in the Canary Islands, REGCAN95, were taken into account (Caturla, 1996). The network was revisited three times (2006, 2007 and 2008), and preliminary results about the network quality and precision were presented by Prieto et al. (2009). GPS coordinates at each epoch were computed using scientific geodetic-precision softwares (GAMIT-GLOBK v10.3 and Bernese v.5.0). Horizontal deformations from the comparison between the 1994 and 2007 epochs are insignificant, but vertical deformations are quite significant (see Fig 9a-b, in Prieto et al., 2009). Comparison between low precision coordinates from the 1994 campaign has limited our interpretation of those results, but assuming that the large source of error between the pair of coordinate sets may be the reference system, inner differences should be smaller than global differences. Taking into account that DInSAR is a relative measurement and we have obtained a zero-deformation rate in the eastern flank of Cumbre Vieja (Fig 5a), we can analyze the differences with respect to the TIRI vertex. The JEDE vertex exhibited a relative vertical motion with respect to TIRI of ~2-3 mm/yr of subsidence, but for both TIME and SANT stations (north and south of the western flank, see Fig 5a) deformation rates are marginal. In Fig. 4b, we show that horizontal components of the motion are not significant for a period of almost

one year between 2006 and 2007 (Prieto et al., 2009). These results suggest that a large part of the ground motion could be vertical.

The terrestrial gravity survey (Camacho et al., 2009) was carried out in June and November 2006 with a LaCoste & Romberg model G gravimeter equipped with a digital recording device. The total number of observations was 385, corresponding to 318 benchmarks. The total amount of redundant observations is about 17% of the total. Simultaneously, elevation values for the benchmarks were determined by means of GPS differential observations with an estimated accuracy of the resulting values that is generally better than 10 cm. By traverse fit we estimate the internal accuracy of the adjusted gravity data as 0.068 mGal (1 mGal=10-5 m s-2).

Gravity values were referred to IGSN71. By combining the gravity and GPS elevation data, we calculated the gravity anomaly. For that, a free-air gradient of -0.308 mGal/m and a value for average density of 2300 kg/m^3 were considered to be applied for the Bouguer correction. Terrain effects were determined from a digital elevation model (DEM) composed by 129000 points. This model is composed of a grid of points, 25 m square, for the terrestrial area plus satellite bathymetry for a distance of 100 km on a 3 km grid, obtained from http://topex.ucsd.edu/cgi-bin/get_data.cgi. Very large correction values for the topographical effects were obtained. They range from 12.5 mGal to 62.4 mGal, with an average value of 26.2 mGal.

By including the terrain correction for the gravity anomaly we computed a Bouguer anomaly (with terrain correction) map (see Fig. S3). Values for Bouguer anomaly are

distributed around an average value of 247.17 mGal with a standard deviation of 25.50 mGal.

4. Geodetic Data modelling

4.1. Ground deformation modelling

We assume that the observed LOS ground deformation (Fig. 5) could be due to deformation or slip on a detachment or weak layer beneath the western flank of Cumbre Vieja that corresponds to either debris avalanche deposits or marine/volcanoclastic sediments (Carracedo et al., 1999; Day et al., 1999a; Urgeles et al., 2000; Ward and Day et al., 2001; Hildenbrand et al., 2003). Here we have modelled the ground deformation using a rectangular dislocation with free dip-slip motion on the fault plane, simulating in a homogeneous, isotropic and elastic half-space a normal fault mechanism (Okada, 1985). Such a modelling approach is convenient for fast evaluation (inverse modelling), but it has several clear disadvantages and can potentially bias our results. It assumes a flat surface, yet topography may play an important role at Cumbre Vieja. To assess the contribution of topography, we evaluated such an effect using the method of Williams and Wadge (1998), which approximates the topographic effect using the variation of depth method. The results indicate that these differences can be as large as ~10%. Heterogeneity of the media also can present a potential bias source (Fernández and Rundle, 1994), but these effects has been demonstrated to be of first order at caldera systems (Manconi et al., 2007), and a minor effect on volcano flanks (Hooper et al., 2002), so the assumption of homogeneity can be accepted.

Stacked average velocity maps result in several thousands of useful data points (Fig. 5a-b), impacting the efficiency of the search for the set of optimal model parameter for the

422 fault plane dislocation. Therefore, it is necessary to reduce this number. In the literature,
423 several algorithms have been proposed to deal with the simplification of the ground
424 deformation, but most are based on a raster-based concepts, regular sampling or quad-
425 tree partitions (Jonsson et al., 2002). Here, we developed a procedure to select the best
426 subset of points that represents the ground deformation pattern using a Triangulated
427 Irregular Network (TIN) instead of a raster (grid). This concept adapts better to an
428 irregular distribution of points, as obtained from advanced DInSAR processing
429 techniques (SBAS or PSI). In our particular case, this approach also adapts better to an
430 irregular coastline contour with striking azimuth. Essentially, it searches for an optimal
431 Delaunay triangulation, where we analyzed the normal distance of each triangle facet to
432 a selected point and this point will be remove from the Delaunay network if the distance
433 is below a specified error threshold (González et al., *in preparation*).
434
435 **FIGURE 6**
436
437 In the search for optimal model parameters, we adopt a non-linear global inversion
438 technique, a bounded simulated annealing (Cervelli et al., 2001), to calculate the best-
439 fitting model that finds the minima in the misfit function in a weighted least square
440 sense. We weighted the TIN-selected data on each period with a variance-covariance
441 matrix constructed with a theoretical covariance function fitted to the empirical
442 covariance function of the stacked data in the northern part of the island (Fig. 6).
443 Determination of the temperature decay function for the simulated annealing is not
444 trivial and there is a likelihood that it will be incorrectly selected, which can result in a
445 failure to find the global minima (Shirzaei and Walter, 2009). For that reason and to
446 evaluate the performance of the algorithm, we started the inversion 500 times with a

447 homogenously distributed random set of initial model parameters. We determined the
448 best-fitting model parameters as the mean of the 500 best-fitting set of model
449 parameters and the associated errors as their standard deviations (Fig. 7).
450
451 **FIGURE 7**
452
453 In Fig. 8, we show the TIN-selected data for both periods (Fig. 8a and 8d), the best-
454 fitting model prediction (Fig. 8b and 8e) and the residuals (Fig. 8c and 8f). The model
455 explains the bulk of the deformation observed in the stacks, but is less accurate in the
456 noisier 2003-2008 period, with a root-mean-square misfit of 1.782 and 2.477 mm/yr for
457 1992-2000 and 2003-2008 periods, respectively. In the 1992-2000 period, it is worth
458 noting the very good fit; despite of the explored simple geometry model and the
459 assumed homogenous slip, only significant spatially correlated residuals occur on the
460 Teneguia area (Fig. 8c). The noisier ground deformation rates for the 2003-2008 period
461 present similar results to the 1992-2000 period. Much larger residuals occur around the
462 Cumbre Vieja, but a significant reduction of the observed deformation occurs in the
463 western flank. This indicates that these results should be carefully used during
464 interpretation. A complete list of results with the best-fitting model parameters and their
465 uncertainties, together with the selected searching bounds used for the inversion, can be
466 found in Table S4.
467
468 **FIGURE 9**
469
470 *4.2. Gravity modelling*

Using the 317 gravity measurements, we performed a nonlinear three-dimensional gravity inversion technique (Camacho et al., 2007), which has been modified to take into account a density increase with depth. This inversion scheme discretizes the subsurface volume and assigns a density contrast, in a fully automatic and non-subjective manner, in a random growth process with respect to a continuous exponentially stratified background. It results in the construction of the geometry of the anomalous density bodies (Camacho et al., 2009). The three-dimensional gravimetric inversion model suggests several structural properties of the island. In the Fig. 9, three profiles where constructed, a N-S profile across the western slopes of Cumbre Vieja (Fig. 9a) and two E-W at the northern (Fig. 9b) and southern (Fig. 9c) section of Cumbre Vieja. In the N-S profile, we can clearly distinguish the high-density body corresponding to the uplifted seamount and the plutonic complex that crops out at the bottom of Caldera de Taburiente, while the southern half of the island, comprised primarily of the Cumbre Vieja series, is characterized by less dense material. Another interesting feature is a discontinuity in the border of the high-density body, which may represent a contrast between different materials, as expected in the buried "Coebra" collapse structure. In the density model, we do not distinguish a density contrast between the volcanic and the pre-volcanic (sedimentary and oceanic-crust) formations, likely related to the loss of resolution with depth of geophysical inversion methods. Finally, in Fig. 9a an important body of low density has been detected beneath western slopes of Cumbre Vieja. Such low density bodies are not only constrained to the western flank of Cumbre Vieja, but it are seen where the anomalies are thicker as well (Fig. S4). We suggest that this body might represent, to some degree, either debris-avalanche and hyaloclastite deposits from Cumbre Nueva collapse or significant deposits of an older sedimentary apron that completely surrounds the high-density core,

or some combination of the two. Their significant thicknesses may be the result of the superposition of a long-term denudation of subaerial material or old collapses from the northern shield volcanoes. E-W profiles seems to indicate that extension diminishes southwards with a relatively larger thickness in the northern part of Cumbre Vieja and smaller amount of material at the southern part of the island. A deeper analysis of the gravimetric data, methods and the structural model can be found in Camacho et al. (2009).

FIGURE 9

5. Discussion

5.1. The relevance of the 1949 summit eruption

The 1949 summit eruption was both qualitatively and quantitatively different from other events in the recent geological history of the island and includes the occurrence of a west-facing 4-km long normal fault scarp (Fig. 3e and Romero-Ortíz and Bonelli-Rubio, 1951; San Miguel de la Cámara et al., 1952; Martel San Gil, 1960; Day et al., 1999a) and the opening of two very sparsely separated effusive vents with chemically different erupted magmas (Klügel et al., 1999). Historical eruptions (< 500 years) has been grouped into the more frequent N-S rift zone eruptions with the opening of roughly N-S oriented vents (1480; 1646; 1677 and 1971), but also those along the summit area and the western flank with opening fissures and vents oriented E-W (1585; 1712 and 1949), an indicator of stress change (Day et al., 1999a). The 1949 event was largely different and a strong indicator of the flank instability, because it was the first faulting event occurring over, at least, a period of some tens of thousands of years (Day et al., 1999a). Even after more than 60 years the fault trace can be recognized in the field (Day et al.,

521 1999a; Carracedo et al., 2001) and using Google Earth©. The mechanism of the faulting
522 has been debated (Klügel et al., 1999), but a certain consensus has been reached about
523 its volcano-tectonic origin (Day et al., 1999a; Hilderbrand et al., 2003).
524
525 *5.2. Structural and morphostructural features*
526 A particularly important feature is the presence of the Cumbre Nueva collapse scar,
527 upon which the Cumbre Vieja volcano is partly built. Apart from the suggestion of
528 several authors, up to now no geophysical evidence corroborated the hypothesis that the
529 scar was infilled by a different low-strength material. Here, we confirm the existence of
530 a thicker body of anomalous mass by means of a gravimetric anomalous density model
531 (Camacho et al., 2009). Also, a recent magnetotelluric survey (García and Jones, 2010)
532 suggests the existence at similar depths of a low-resistivity body, which also confirms
533 that scuh hypothesis is correct and the Cumbre Vieja volcano series rests on the remains
534 of the collapsed Cumbre Nueva ridge (a breccoid layer). In Fig. 10, we show the
535 morphology of the low density body at depth and the extension. The anomaly aligns
536 with the region of the maximum vertical deformation region of both DInSAR stacks
537 (Fig. 5). The low density body also is spatially coincident in its depth range with the
538 modelled fault planes (rectangles on Fig. 10). Despite the assumptions used in these
539 simple models, gravimetric inversions and ground deformation modelling (half-space)
540 results suggest a depth range for the detachment fault of 2-4 km depths. Those results
541 are consistent with the lower bounds of possible intravolcanic structures, such as the
542 Cumbre Nueva collapse scar (debris avalanche process), or the very upper depth limits
543 for the contact between pre-volcanic sediments and island-volcanics (slumping process).
544 Unfortunately, we are not able to resolve the depth range more accurately using
545 geodetic data alone, so we cannot rule out the possibility of a fault located at the contact

546 between prevolcanic material and the volcanic series or at the shallower levels.
547 Additional investigations should be carried out to better constrain this aspect.
548
549 **FIGURE 10**
550
551 Additional insights into the long-term dynamics of the flank can be obtained from
552 geomorphologic analysis. Topographic bulges and/or plateaus are commonly associated
553 with deformation processes at active volcanoes (Wooler et al., 2004; Márquez et al.,
554 2008). In particular, a morphological analysis of the local topography suggests the
555 presence of topographic anomalies in several E-W profiles across the Cumbre Vieja,
556 attributed to active volcano-tectonic processes (see Fig. 5 in Hildenbrand et al., 2003),
557 which also are spatially coincident with the mapped deformation (Fig. 5 and 10). In
558 addition, a clear open westward bending structure (Fig. 10) drawn from the outline of
559 the last eruptions (Guillou et al., 1998) may reflect sliding on a gently sloping structure
560 at depth (Wooler et al., 2004). However, it should be noted that, as in the case of the
561 mobile south flank of Kilauea, no shear (strike-slip) structures are recognized onshore at
562 the north and south boundaries of the deformation area, probably due to the limited
563 movement of such structures (Denlinger and Okubo, 1995).
564
565 *5.3. On-going deformation and its implications for steep-side volcano flanks*
566 The observed volcanic ground deformation can be caused by a broad range of
567 mechanisms: *a)* changes in the pore-pressure of shallow aquifers produce measurable
568 ground deformation at similar rates elsewhere in the Canary Islands (Fernández et al.,
569 2005). However, although the Cumbre Vieja aquifer has high permeability, it is not
570 used for groundwater abstraction for water supply due to its high salinity as a result of

571 volcanic CO_2 enrichment (pp. 16292 *in* Plan Hidrológico Insular de La Palma, 2001). *b)*
572 Deformation due to lava compaction or loading should also be restricted to areas
573 covered by or adjacent to recent lava flows, but that is not the case in this region (Fig.
574 5). The spatial wavelength of the signal (~8 km in the N-S direction) also does not
575 support very deep magmatic sources, such as petrologically inferred magma chambers
576 at mantle depths (Klügel et al., 2005). Finally, *c)* ground deformation due to the
577 emplacement of shallow intrusions likely occurs only during unrest periods
578 accompanied by felt seismicity, which also is not the case for the 1992-2008 period.
579
580 In general, ground deformation is accompanied by seismicity, but it is noteworthy that
581 at La Palma seismicity is lacking completely, with no seismic events recorded inside or
582 in the close vicinity of the island in the past 20 years
583 (http://www.ign.es/ign/en/IGN/SisCatalogo.jsp). This may be due, in part, to the poor
584 spatial coverage of the national seismic network, with only two operating seismographs
585 (http://www.ign.es/ign/home/geofisica/sismologia/mapaEstaciones.jsp). Another likely
586 possibility is that seismic events are not occurring on well-defined seismic faults, which
587 radiate enough seismic energy to be recorded at nearby stations. Instead, creeping
588 processes with associated non-volcanic tremor may release the stress on the sliding
589 surfaces, a process that potentially can remain undiscovered without dedicated seismic
590 observations.
591
592 The smoothness and spatial distribution of our geodetic results (Fig. 5) suggests that the
593 detachment fault is slow stable-sliding at depth beneath the western flank of the edifice
594 in the on- and offshore region close to the shoreline, on a fault segment with creeping
595 friction properties (Fig. 10). This behaviour is likely steady-state, or might be

596 punctuated by unobserved slow-slip events, in the transition zone between frictionally
597 different segments of the developing fault surfaces (Segall et al., 2006; Brooks et al.,
598 2006). Only during eruptions, the slip could be able to propagate into immature, stick-
599 slip frictional fault segments, as ruptured during the 1949 eruption. The possibility of a
600 similar event during the next summit eruption should be inferred with caution (Ward
601 and Day, 2001), as only optimally located and oriented dike intrusions will result in
602 encouragement of the slip on the detachment fault, as suggested by recent results of
603 stress transfer at volcanoes (Walter et al., 2005; Amelung et al., 2007).
604
605 We also speculate that the on-going creeping processes, acting at the base of the western
606 flank, may contribute to the equilibrium of the anomalous gravitational potential energy
607 of the flank masses, reducing the landslide risk, as long as the bulk cohesion of the
608 material remains stable. However, the exact mechanism of stress dissipation at the
609 sliding area/surfaces could greatly differ from this process (e.g., progression from creep
610 to more stable sliding/failure in favour of weak layers or well oriented structure/mineral
611 fabrics). Dilatational stresses due to shallow dike intrusion along the rift-zone, fluid
612 injection or groundwater pressurization (Elsworth and Voight, 1995) will promote
613 reduction of the friction angle on the sliding surfaces, which in turn can result in the
614 acceleration of the slumping structure. However, a potential collapse seems to be a
615 more remote possibility, due to *a)* the relatively low variance of the volume of Cumbre
616 Vieja volcanic edifice during the last 7 ka (a period with several summit eruptions), *b)*
617 the immature geomorphologic/topographic expression of the fault at the surface, and *c)*
618 the relatively gentle slopes in comparison with more steep-sided volcanoes (e.g., Fogo
619 (Cape Verde), Pico (Açores), Teide (Tenerife) which exhibit greater slopes, Fig. S1).
620

6. Conclusions

In this work, we report a slow subsidence rate on the western flank of Cumbre Vieja volcano detected using InSAR data, and a prominent low density zone identified using a new gravity structural model. Elastic modelling of the radar data could explain observed deformation with slip on an active creeping detachment surface that fits the contour of the low density zone (Fig. 10). Spatial coalescence of *a)* a prominent volcano edifice underlain by a ductile layer (old sediments or debris avalanche deposits), *b)* a buried buttress structure in the eastern flank and *c)*, concentrated westwards dilatational magmatic stresses due to repeated N-S rift intrusions in the last 7 ka results in the initiation and progressive development of an active aseismic mobilisation of the western flank. We conclude that the detachment layer may act as an efficient boundary for the aseismic stress release due to gravitational loading during intereruptive periods (present activity), encouraging dike intrusions at the N-S rift zone. The release of dilatational magmatic stresses during these N-S rift intrusions encourages slip and promotes high-angle normal faulting at the border of the slip area (1949 eruption), reorienting the stress field around the volcano and resulting in near E-W fissural eruptions in the western flank. This simple model satisfactorily explains the ground deformation data and also complements the geological and geophysical evidence that Cumbre Vieja volcano is in an early state of an immature collapsing process (< 20-7 ka). We also speculate that ongoing creeping beneath the western flank of Cumbre Vieja tends to stabilize the flank through reorganization and a decrease of gravitational potential forces. In any case, this conclusion does not preclude that any sudden and/or unusual change in the stress field, such as a dike intrusion or groundwater pressurization, could trigger a catastrophic collapse.

646 We want to emphasize, based on our results, the potential of stacked InSAR data to
647 measure subtle deformation rates at volcano flanks, even in the absence of clear seismic
648 evidence of magmatic or volcano-tectonic activity. Our results support the proposition
649 that volcano-tectonism and the present and recent past volcanic activity are intimately
650 related at La Palma and may help the evaluation of the hazard related to a future
651 eruption. We also envisage that the characterization of volcano-tectonic deformation
652 process will contribute to any quantitative parameterization analysis of tsunamigenic
653 studies at La Palma (Ward and Day, 2001; McGuire, 2006). Finally, the intensification
654 of ground deformation measurements and a possible near-real time geodetic monitoring
655 system is crucial on this specific volcano flank and would contribute significantly to the
656 understanding of the associated hazard specifically and volcano flank dynamics in
657 general.
658

Acknowledgements

Our research was supported in part by the Spanish MICINN projects: GEOMOD (CGL2005-05500-C02), PEL2G (CGL2008-06426-C01-01/BTE), PCI2006-A7-0660, and also the ECGS-funded "*Space geodesy by means of SAR Interferometry (InSAR) at the pan-African continental rifting zone: from local-scale volcanism to plate-scale deformation*". Data were kindly provided by ESA, through CAT1:2679, DECIDE Volcano and ALOS/ADEN-AO3690 projects. We are indebted to Ayuntamiento de Fuencaliente and Parque Nacional de la Caldera de Taburiente. PJG was partially funded by a UCM PhD Thesis Research Fellowship. The research of KFT was supported by an NSERC Discovery Grant. GMT tools (Wessel and Smith, 1998) were used to create (2, 3, 5, 7 and 10 figures and partly 9) and Matlab for create figures 4, 6 and 8. This work contains results from the Ph.D. Thesis of PJG. This work has been partially done in the frame of the Moncloa Campus of International Excellence (UCM-UPM, CSIC).

References

Amelung, F., Jonsson, S., Zebker H.A. Segall, P., 2000. Widespread uplift and trap door faulting on Galápagos volcanoes observed with radar interferometry. Nature, 407, 993-996.

Amelung, F., Yun, S-H., Walter, T.R., Segall, P. Kim, S.W., 2007. Stress control of deep rift intrusion at Mauna Loa volcano, Hawaii. Science 316, 1026-1030, doi:10.1126/science.1140035.

Ancoechea, E., Hernán, F., Cendrero, A., Cantagrel, A., Fuster, J.M., Ibarrola, E., Coello J., 1994. Constructive and destructive episodes in the building of a young oceanic islands. La Palma Canary Islands and genesis of the Caldera de Taburiente, J. Volcanol. Geotherm. Res. 60, 243–622.

Anderssohn, J., Motagh, M., Walter, T.R., Roseneau, M., Kaufmann, H., Oncken, O., 2009. Surface deformation time series and source modeling for a volcanic complex system based on satellite wide swath and image mode interferometry: The Lazufre system, central Andes. Remote Sensing of Environment, 113, 2062–2075, doi:10.1016/j.rse.2009.05.004.

Barzaghi, R., Sansò, F., 1983. Sulla stima empirica della funzione di covarianza. Boll. Di Geod. E Sci. Affini, 4, 389-415.

Brooks, B.A., Foster, J.H., Bevis, M., Frazer, L.N., Wolfe, C.J., Behn, M., 2006. Periodic slow earthquakes on the flank of Kīlauea volcano, Hawai'i, Earth Planet. Sci. Lett. 246, 207-216, doi:10.1016/j.epsl.2006.03.035

Brooks, B.A., Foster, J., Sandwell, D., Wolfe, C.J., Okubo, P., Poland, M., Myer, D., 2008. Magmatically triggered slow slip at Kilauea volcano, Hawaii, Science 321, 1177, doi:10.1126/science.1159007.

Camacho, A.G., Nunes, J.C., Ortiz, E., Franca, Z., Vieira, R., 2007. Gravimetric determination of an intrusive complex under the island of Faial (Azores): Some methodological improvements, Geophys. J. Int., 171, 478-494, doi:10.1111/j.1365-246X.2007.03539.x.

Camacho, A.G., Fernández, J., González, P.J., Rundle, J.B., Prieto, J.F., Arjona, A., 2009. Structural results for La Palma Island using 3-D gravity inversion, J. Geophys. Res. 114 (B5), doi: 10.1029/2008JB005628.

Carracedo, J.C., 1999. Growth, structure, instability and collapse of Canarian volcanoes and comparisons with Hawaiian volcanoes, J. Volcanol. Geoth. Res. 94 (1–4), 1-19.

Carracedo, J.C., Day, S., Guillou, H., Rodríguez Badiola, E., Canas J.A., and Pérez Torrado, F.J., 1998. Hotspot volcanism close to a passive continental margin: the Canary Islands. Geol. Mag., 135, 591-604.

Carracedo, J.C., Day, S.J., Guillou, H., Pérez Torrado, F.J., 1999. Giant quaternary landslides in the evolution of La Palma and El Hierro, Canary Islands, J. Volcanol. Geoth. Res. 94 (1–4), 169-190.

Carracedo, J.C., Badiola, E.R., Guillou, H., De la Nuez, J., Pérez Torrado, F.J., 2001. Geology and volcanology of La Palma and El Hierro, Western Canaries. Estudios Geol., 57, 175–273. doi:10.3989/egeol.01575-6.

Casu, F., Manzo, M., Lanari, R., 2006. A quantitative assessment of the SBAS algorithm performance for surface deformation retrieval from DInSAR data, Remote Sensing Environ., 102, 3-4, 195-210. doi:10.1016/j.rse.2006.01.023

Caturla, J.L., 1996. REGCAN95, Nueva Red Geodésica de las Islas Canarias., Instituto Geográfico Nacional, Área de Geodesia. Internal Report. (*in Spanish*).

Cavalié, O., Doin, M.P., Lasserre, C., Briole, P., 2007. Ground motion measurement in the Lake Mead area, Nevada, by differential synthetic aperture radar interferometry time series analysis: probing the lithosphere rheological structure. J. Geophys. Res. 112 (B3), B03403. doi:10.1029/2006JB004344.

Cervelli, P., 2004. The Threat of Silent Earthquakes, Scientific American.

Cervelli, P., Murray, M. H., Segall, P., Aoki, Y., Kato, T., 2001. Estimating source parameters from deformation data, with an application to the March 1997 earthquake swarm off the Izu Peninsula, Japan. J. Geophys. Res. 106, 11217-11238.

Cervelli, P., Segall, P., Johnson, K., Lisowski, M., Miklius, A., 2002. Sudden aseismic fault slip on the south flank of Kilauea volcano, Nature 415 (6875), 1014-1018.

Clague, D.A., Denlinger, R.P., 1994. Role of olivine cumulates in destabilizing the flanks of Hawaiian volcanoes. Bull. Volcanol. 56, 425-434.

Colesanti, C., Wasowskia, J., 2006. Investigating landslides with space-borne Synthetic Aperture Radar (SAR) interferometry, Engineering Geology, 88 (3-4), 173-199, doi:10.1016/j.enggeo.2006.09.013.

731 Day, S.J., Carracedo, J.C., Guillou, H., 1997. Age and geometry of an aborted rift flank collapse: the San
732 Andres fault, El Hierro, Canary Islands. Geol. Mag. 134, 523-537.
733 Day, S., Carracedo, J.C., Guillou, H., Gravestock, P., 1999a. Recent structural evolution of the Cumbre
734 Vieja Volcano, La Palma, Canary Islands: Volcanic rift zone reconfiguration as a precursor to
735 volcanic flank instability? J. Volcanol. Geotherm. Res., 94 (1-4), 135-167.
736 Day, S.J., Heleno da Silva, S.I.N., Fonseca, J.F.B.D., 1999b. A past giant lateral collapse and present-day
737 flank instability of Fogo, Cape Verde Islands. J. Volcanol. Geotherm. Res. 94 (1-4), 191-210.
738 de la Nuez, J., 1984. El Complejo intrusivo subvolcánico de la Caldera de Taburiente, Ph.D. thesis, 401
739 pp., Universidad Complutense de Madrid. *(in Spanish)*
740 Denlinger, R.P., Okubo, P., 1995. Structure of the mobile south flank of Kilauea volcano, Hawaii, J.
741 Geophys. Res., 100, 24499-24507.
742 Doin, M.-P., Lasserre, C., Peltzer, G., Cavalié, O., Doubre, C., 2009. Corrections of stratified
743 tropospheric delays in SAR interferometry: Validation with global atmospheric models, Journal
744 of Applied Geophysics 69, 35–50, doi:10.1016/j.jappgeo.2009.03.010
745 Duffield, W.A., Stieltjes, L., Varet, J., 1982. Huge Landslide blocks in the growth of Piton de la
746 Fournaise, La Reunion, and Kilauea Volcano, Hawaii. J. Volcanol. Geotherm. Res. 12, 147–160.
747 Eff-Darwich, A., García-Lorenzo, B., Pérez-Darias, J.C., González, A., Fernández, J., González, P.J.,
748 2009. Characterization of the distribution of water vapour for DINSAR studies on the volcanic
749 island of Tenerife, Canary Islands, In proceedings: SPIE's Europe Remote Sensing International
750 Symposium, 31 August-3 September 2009, Berlin (http://spie.org/remote-sensing-europe.xml).
751 Elsworth, D., Voight, B., 1995. Dike intrusion as a trigger for large earthquakes and the failure of volcano
752 flanks, J. Geophys. Res. 100, 6005-6024.
753 Fernández, C., de la Nuez, J, Casillas, R., García Navarro, E., 2002a. Stress fields associated with the
754 growth of a large shield volcano (La Palma, Canary Islands), Tectonics, 21(4),
755 doi:10.1029/2000TC900038.
756 Fernández, J., Romero, R., Carrasco, D., Luzón, F., Araña, V., 2002b. InSAR volcano and seismic
757 monitoring in Spain. Results for the period 1992–2000 and possible interpretations, Opt. Lasers
758 Engin. 37, 285-297.

759 Fernández, J., Romero, R.; Carrasco, D., Tiampo, K.F., Rodríguez-Velasco, G., Aparicio, A., Araña, V.,
760 González-Matesanz, F.J., 2005. Detection of displacements in Tenerife Island, Canaries, using
761 radar interferometry, Geophys. J. Int., 160, 33-45.
762 Fernández, J., and Rundle, J.B., 1994. Gravity changes and deformation due to a magmatic intrusion in a
763 two-layered crustal model, J. Geophys. Res., 99, 2737-2746.
764 Fialko, Y., 2006. Interseismic strain accumulation and the earthquake potential on the southern San
765 Andreas fault system, Nature, 441, 968-971, doi:10.1038/nature04797.
766 Foster, J., B. Brooks, T. Cherubini, C. Shacat, S. Businger, and C. Werner (2006), Mitigating atmospheric
767 noise for InSAR using a high resolution weather model, Geophys. Res. Lett., 33, L16304,
768 doi:10.1029/2006GL026781.
769 Froger, J.L., Merle, O., Briole, P., 2001. Active spreading and regional extension at Mount Etna imaged
770 by SAR interferometry. Earth Planet. Sci. Lett. 148, 245-258.
771 García, X., A.G. Jones, 2010. Internal structure of the western flank of the Cumbre Vieja volcano (La
772 Palma, Canary Islands) from land magnetotelluric imaging, J. Geophys. Res.,
773 doi:10.1029/2009JB006445.
774 Guillou, P.-Y., Carracedo, J.C., Day, S.J., 1998. Dating of the Upper Pleistocene-Holocene volcanic
775 activity of La Palma using the unspiked K-Ar technique, J. Volcanol. Geotherm. Res. 86, 137–
776 149, doi:10.1016/S0377-0273(98)00074-2.
777 Guillou, H., Carracedo, J.C., Duncan, R.A., 2001. K-Ar, 40Ar-39Ar ages and magnetostratigraphy of
778 Brunhes and Matuyama lava sequences from La Palma Island. J. Volcanol. Geotherm. Res.,
779 106(3-4), 175-194, doi:10.1016/S0377-0273(00)00294-8
780 Hanssen, R.F., 2001. Radar interferometry: Data interpretation and error analysis, Kluwer Academic
781 Publishers, Dodrecht, The Netherlands. 328 pp.
782 Hildenbrand, A., Gillot, P.-Y., Soler, V., Lahitte, P., 2003. Evidence for a persistent uplifting of La Palma
783 (Canary Islands), inferred from morphological and radiometric data, Earth Planet. Sci. Lett. 210,
784 277–289.
785 Holcomb, R.T., Searle, R.C., 1991. Large landslides from oceanic volcanoes. Marine Geotechnology 10,
786 19-32.
787 Hooper, A., Segall, P., Johnson K., Rubinstein J., 2002. Reconciling seismic and geodetic models of the
788 1989 Kilauea south flank earthquake, Geophys. Res. Lett., 29, doi:10.1029/2002GL016156.

789 Johansen, T.S., Hauff, F., Hoernle, K., Klügel, A. and Kokfelt, T.F., 2005. Basanite to phonolite
790 differentiation within 1550-1750 yr: U-Th-Ra isotopic evidence from the A.D. 1585 eruption on
791 La Palma, Canary Islands, Geology, 33(11), 897-900, doi:10.1130/G21663.1.
792 Jonsson, S., Zebker, H., Segall, P., Amelung, F., 2002. Fault slip distribution of the 1999 Mw 7.1 Hector
793 Mine, California, earthquake, estimated from satellite radar and GPS measurements, Bull. Seism.
794 Soc. Am. 92 ,1377-1389.
795 Kampes, B.M., Hanssen, R.F., Perski, Z., 2003. Radar Interferometry with Public Domain Tools
796 Proceedings of the FRINGE 2003 Workshop, Frascati, Italy, 6 pp.
797 Klügel, A., Schmincke, H.U., White, J.D.L., Hoernle, K.A., 1999. Chronology and volcanology of the
798 1949 multi-vent rift-zone eruption on La Palma (Canary Islands). J. Volcanol. Geotherm. Res.
799 94, 267–282.
800 Klügel, A., Hansteen, T.H., Galipp, K., 2005. Magma storage and underplating beneath Cumbre Vieja
801 volcano, La Palma (Canary Islands), Earth Planet. Sci. Lett. 236, 211–226.
802 Lipman, P.W., Mullineaux, D.R., 1981. The 1980 eruptions of Mount St. Helens, Washington: U.S.
803 Geological Survey Professional Paper 1250, 844 pp.
804 Lundgren, P. Berardino, P., Coltelli, M., Fornaro, G., Lanari, R., Puglisi, G., Sansosti, E., Tesauro, M.,
805 2003. Coupled magma chamber inflation and sector collapse slip observed with SAR
806 interferometry on Mt. Etna volcano, J. Geophys. Res. 108, 2247-2261.
807 Manconi, A., Walter, T. R., F. Amelung, (2007). Effects of mechanical layering on volcano deformation.
808 *Geophys. J. Int.*, 170, 952-958.
809 Márquez, A., López, I., Herrera, R., Martín-González, F., Izquierdo, T. Carreño, F. Spreading and
810 potencial instability of Teide volcano, Tenerife, Canary Islands, 2008. Geophys. Res. Lett.
811 35(L05305), doi:10.1029/2007GL032625.
812 Martel San Gil, M., 1960. El volcán de San Juan, también llamado de “Las Manchas” y del
813 “Nambroque”. La Palma (Canarias), Madrid. *(in Spanish)*
814 Masson, D.G., 1996. Catastrophic collapse of the flank of El Hierro about 15,000 years ago and the
815 history of large flank collapses in the Canary Islands. Geology 24, 231–234.
816 Masson, D.G., Watts, A.B., Gee, M.J.R., Urgeles, R., Mitchell, N.C., Le Bas, T.P., Canals, M., 2002.
817 Slope failures on the flanks of the western Canary Islands, Earth-Science Reviews 57, 1-35.

818 Masson, D.G., Harbitz, C.B., Wynn, R.B., Pedersen, G., Lovholt, F., 2006. Submarine landslides:
819 processes, triggers and hazard prediction, Phil. Trans. R. Soc. A, 364, 2,009-2039,
820 doi:10.1098/rsta.2006.1810
821 Massonet, D. Sigmundsson, F. (2000), Remote sensing of volcano deformation by radar interferometry
822 from various satellites. In (Mouginis-Mark, P. J., Crisp, J. A., and Fink, J. H., eds.) Remote
823 Sensing of Active Volcanism, Geophysical Monographs 116, pages 228, 207–221. AGU,
824 Washington DC.
825 McGuire, W.J., 1996. Volcano instability: a review. In: McGuire, W.J., Jones, A.P., Neuberg, J.Ž Eds..,
826 Volcano Instability on the Earth and Other Planets. Geological Society Special Publication,
827 Geological Society of London, London, pp. 1–23.
828 McGuire, W.J., 2006. Global risk from extreme geophysical events: threat identification and assessment,
829 Phil. Trans. R. Soc. A, 364, 1,889-1909, doi:10.1098/rsta.2006.1804
830 Moore, J.G., Clague, D.A., Holcomb, R.T., Lipman, P.W., Normark, W.R. Torresan, M.E., 1989.
831 Prodigious submarine landslides on the Hawaiian Ridge. J. Geophys. Res. 94, 17,465-17,484.
832 Moore, J.G., Normark, W.R., Holcomb, R.T., 1994. Giant Hawaiian Landslides. Annu. Rev. Earth Planet.
833 Sci. 22, 119–144.
834 Moss, J., McGuire, W., Page, D. (1999), Ground deformation monitoring of a potential at La Palma,
835 Canary Islands, J. Volcanol. Geotherm. Res. 94, 251–265.
836 Okada, Y., 1985. Surface deformation due to shear and tensile faults in a half-space, Bull. Seism. Soc.
837 Am. 75, 1135-1154.
838 Owen, S., P. Segall, J. Freymueller, A. Miklius, R. Denlinger, T. Arnadottir, M. Sako, R. Bürgmann,
839 1995. Rapid deformation of the south flank of Kilauea Volcano, Hawaii, Science, 267, 1328-
840 1332.
841 Owen, S., Segall, P., Lisowski, M., Miklius, A., Denlinger, R., Sako, M., 2000. Rapid deformation of
842 Kilauea volcano: global positioning system measurements between 1990 and 1996, J. Geophys.
843 Res., 105(B8), 18983-18998.
844 Perlock P.A., Gonzalez P.J., Tiampo K.F., Rodriguez-Velasco G., Samsonov S. Fernandez J., 2008. Time
845 evolution of deformation using Time Series of differential interferograms: Application to La
846 Palma Island (Canary Islands), Pure and Applied Geophysics, 165(8), 1531-1554,
847 doi:10.1007/s00024-004-0388-7.

Plan Hidrológico Insular de La Palma, 2001. http://www.lapalmaaguas.es/index.php?option=com_content&task=view&id=32&Itemid=83 (*in Spanish*).

Prieto J.F., Gonzalez P. J., Seco A., Rodriguez-Velasco G., Tunini L., Perlock P.A., Arjona A., Aparicio A., Camacho A.G., Rundle J.B., Tiampo K.F., Pallero J.L.G., Pospiech S. Fernandez J., 2009. Geodetic and structural research in La Palma Island, Canary Islands, Spain: 1992-2007 results. Pure and Applied Geophysics, 166, 1461-1484, doi:10.1007/s00024-009-0505-2.

Romero-Ortíz, J., Bonelli-Rubio, J.M., 1951. La erupción del Nambroque (Junio-Agosto de 1949). Talleres del Instituto Geográfico y Catastral. Comisión Nacional de Geodesia y Geofísica. Madrid. *(in Spanish)*

San Miguel de la Cámara, M., Fúster Casas, J.M. Martel M., 1952. Las erupciones y materiales arrojados por ellas en la Isla de La Palma- Junio-Julio de 1949. Bull. Volc., 18 pp. *(in Spanish)*

Sandwell, D.T., Price, E., 1998. Phase gradients approach to stacking interferograms, J. Geophys. Res., 103(B2), 30183-30204.

Segall, P., Desmarais, E.K., Shelly, D., Miklius, A., Cervelli, P., 2006. Earthquakes triggered by silent slip events on Kilauea volcano, Hawaii, Nature 442, doi:10.1038/nature04938.

Shirzaei, M., Walter, T.R., 2009. Randomly iterated search and statistical competency as powerful inversion tools for deformation source modeling: Application to volcano interferometric synthetic aperture radar data, J. Geophys. Res., 114, B10401, doi:10.1029/2008JB006071.

Staudigel, H., Feraud, G., Giannerini, G., 1986. The history of intrusive activity on the Island of La Palma (Canary Islands), J. Volcanol. Geotherm. Res. 27, 299-322.

Urgeles, R., Masson, D.G., Canals, M., Watts, A.B., Le Bas, T., 1999. Recurrent large-scale landsliding on the west flank of La Palma, Canary Islands. J. Geophys. Res., 104, 25331-25348.

Urgeles, R., Canals, M., Roberts, J., and the SNV "Las Palmas" shipboard party, 2000. Fluid flow from pore pressure measurements off La Palma, Canary Islands. J. Volcanol. Geotherm. Res. 101, 253-271.

Walter T.R., Acocella, V., Neri, M., Amelung, F., 2005. Feedback processes between magmatic events and flank movement at Mount Etna (Italy) during the 2002–2003 eruption, J. Geophys. Res., 110, B10205, doi:10.1029/2005JB003688.

Ward, S.N., 2002, Slip-sliding away, Nature, 415, 973-974.

878 Ward, S.N. Day, S. J. (2001), Cumbre Vieja volcano-potencial collapse and tsunami at La Palma, Canary
879 Islands, Geophys. Res. Lett. 28(17), 3397–3400.
880 Wessel, P., Smith, W.H.F., 1998. New, improved version of Generic Mapping Tools released, EOS
881 Trans. Am. Geophys. Union, 79, 579.
882 Wooller, L.K., van Wyk de Vries, B., Murray, J.B., Rymer, H., Meyer, S., 2004. Volcano spreading
883 controlled by dipping substrata, Geology, 32 (7), 573-576.
884 Wright, T., Parsons, B. Fielding, E., 2001. Measurement of interseismic strain accumulation across the
885 North Anatolian Fault by satellite radar interferometry, Geophys. Res. Lett., 28(10), 2117-2120.
886 Wright, T.J., Parsons, B., England, P.C. Fielding, E.J., 2004. InSAR observations of low slip rates on the
887 major faults of western Tibet, Science, 305(5681), 236-239.
888 Wynn, R.B., Masson, D.G., 2003. Canary Islands landslides and tsunami generation. In, Locat, J. and
889 Mienert, J. (eds.) Submarine mass movements and their consequences: 1st International
890 Symposium. Dordrecht, Netherlands, Kluwer Academic, 325-332. (Advances in Natural and
891 Technological Hazards Research 19).
892
893

894 **List of Figures:**

895

896 **Figure 1.** Sketch of shallow vs. deep flank motion (a) Kilauean-like unstable volcanoes
897 and (b) Macaronesian-like unstable volcanoes. See also the Fig. S1 and its caption for a
898 non-comprehensive list of identified unstable flanks at ocean-island volcanoes in the
899 supplementary material. m.s.l stands for mean sea level.

900

901 **Figure 2.** Overview of the main geologic features of La Palma, after the geologic map
902 of Carracedo et al., (2001). Black color shows the outcrop area of the submarine and
903 intrusive complex under the northern shield volcanoes (dark blue colours). After the
904 occurrence of the Cumbre Nueva collapse (discontinuous black line), the Bejenado
905 stratovolcano began to grow, filling the scar (light blue colour). Finally, Cumbre Vieja
906 volcanism (orange colour) developed a prominent NS rift volcano at the southern part of
907 the Island, where current volcanic activity concentrates (historic lava flows in red).
908 White dots show the location of the GPS monitoring network established in 2006
909 (Prieto et al., 2009).

910

911 **Figure 3.** Evolution of the volcano-structural lineaments features at Cumbre Vieja
912 volcano. a) Spatial distribution of the vents and fractures associated with the early
913 period of the Cumbre Vieja construction (125-20 kyr) (modified from Fig 4 in Day et
914 al., 1999a). b) Spatial distribution of the vents and fractures associated with the NE high
915 production period (20-7 kyr) (modified from Fig. 5 in Day et al., 1999a). c) Recent lava
916 flows from historic and sub-historic eruption events (modified from Fig. 6 in Day et al.,
917 1999a). d) Fracture developed during the 1949 summit eruption on 2-3 July (modified
918 from Geological map of La Palma in Carracedo et al., 2001). e) 1949 normal surface

ruptures at Llano del Banco (1949-contemporaneous Mr. Bonelli-Rubio photograph) with estimated throw-slip around one-half to one meter from comparison to pine-trees at the background, which have been estimated at 10 to 15 m in height.

Figure 4. Error analysis on each interferogram that was used in both stacks. a) All (81) empirical spatial covariance functions of the ERS interferograms, b) histogram of all interferograms (gray color) and those used in the ERS period stack (black color), c) all (18) empirical spatial covariance functions of the ENVISAT interferograms, and d) histograms of all interferograms (gray color) and those used in the ENVISAT period stack (black color). Ifgs means for interferograms.

Figure 5. Stack results shown onto a shaded DEM. Differential interferograms were corrected for atmospheric elevation-phase dependence. Results are only from coherent points (pixels), which exhibit LOS linear velocity (positive away from satellite, indicated with the arrows). a) Stacking of 82 long temporal separation ERS differential interferograms for the period 1992-2000, accompanied by vertical GPS linear velocity between 1994 and 2007. b) Stacking of 18 long temporal separation ENVISAT differential interferograms for the period 2003-2008. We also show estimates of horizontal GPS linear velocities between 2006 and 2007. Note the linear rate from 2003-2008 results is noisier than the 1992-2000 results, mainly due to the smaller dataset, so these results should be considered with caution. The largest magnitude subsidence signal corresponds to the Teneguia volcano (T symbol).

943 **Figure 6.** a) Empirical and best-fitting covariance function for the ERS stack. b)
944 Empirical and best-fitting covariance function for the ENVISAT stack. The theoretical
945 covariance function used in the study is in the form of $cov(d) = a\ J_o\ (cd)\ e^{-bd}$, where
946 $J_o(\cdot)$ is the zero-order Bessel function and is a, b and c are constant parameters
947 (Barzaghi and Sansò, 1983). c) The variance-covariance function from the fitted
948 covariance function for the 454 TIN-selected points for the ERS period. d) The
949 variance-covariance function from the fitted covariance function for the 1019 TIN-
950 selected points for the ENVISAT period. Note the different level of noise in the period
951 1992-2000 and 2003-2008 and also the variance reduction after application of the
952 stacking methodology (Fig. 4).
953
954 **Figure 7.** Results of the inversion of the InSAR data from Cumbre Vieja (a and d),
955 using a dislocation model (b and e) (see Table S4 for the corresponding source
956 parameters), where (b) and (e) represents the best-fitting modelled LOS displacement
957 rates. (c) and (f) Residual LOS displacements after subtracting the model from the data.
958 Modelling results in the upper row correspond to the 1992-2000 period and lower row
959 to 2003-2008 period.
960
961 **Figure 8.** a) Histograms of the best-fitting parameters and the root mean square of the
962 weighted residuals for the ERS period (1992-2000) stack. b) Histograms of the best-
963 fitting parameters and the root mean square of the weighted residuals for the ENVISAT
964 period (2003-2008) stack.
965
966 **Figure 9.** Interpreted profiles across the anomalous density inverse gravimetric model.
967 Colours indicate density contrast, blue colours are lower density contrast (min = -306

968 kgr/m^3) and red colours are upper density (max = 351 kg/m^3). a) North-South profile. b)
969 West-East profile at 3167500 UTM Northing coordinate, and c) West-East profile at
970 3160000 UTM Northing coordinate. Note the anomalous low density body beneath the
971 western flank of Cumbre Vieja tends to diminish in extension southward. The axis units
972 are distance in kilometres. Non-interpreted profiles and a horizontal section at -2000 m.
973 bsl are showing the density contrasts. The location of the profiles can be found in the
974 supplementary material (Fig. S3 and S4).
975
976 **Figure 10.** Surface projection of: the best-fitting fault models, for the period 1992-2000
977 (black rectangle) and 2003-2008 (white rectangle); the 1949 normal-faulting surface
978 ruptures (black line); the density contrasts of -150 Kgr/m^3 (blue line) and 150 Kgr/m^3
979 (red line) at a depth of 3000 m. bsl. Interpreted bend area shown with a high density of
980 effusive centers and vents related to the activity of the growing detachment surface.

Figure 1

Click here to download Figure: Figure1.pdf

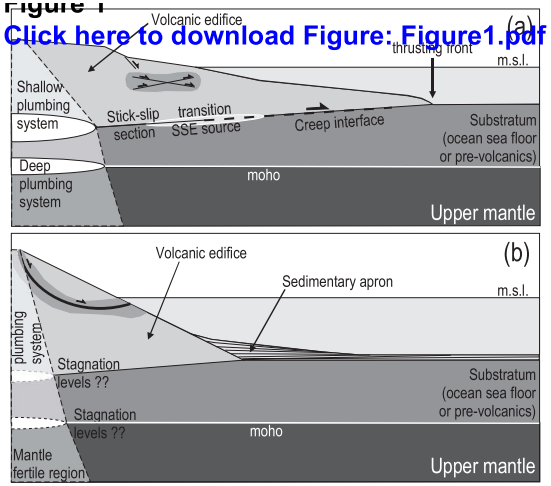

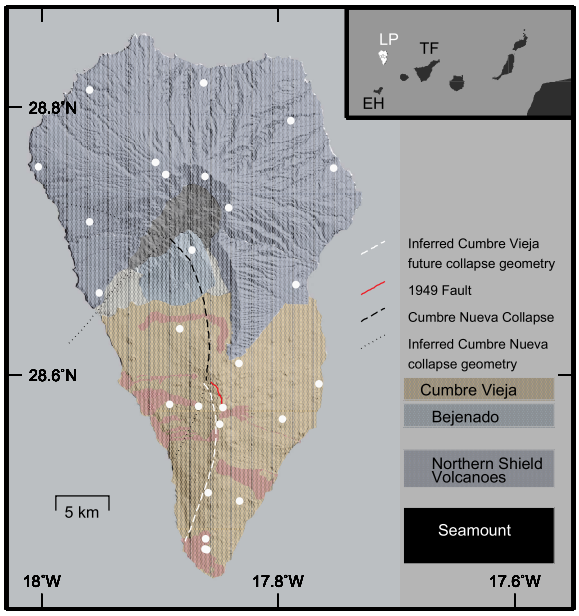
LP
TF
EH
28.8°N
28.6°N
5 km
18°W
17.8°W
17.6°W
Inferred Cumbre Vieja future collapse geometry
1949 Fault
Cumbre Nueva Collapse
Inferred Cumbre Nueva collapse geometry
Cumbre Vieja
Bejenado
Northern Shield Volcanoes
Seamount

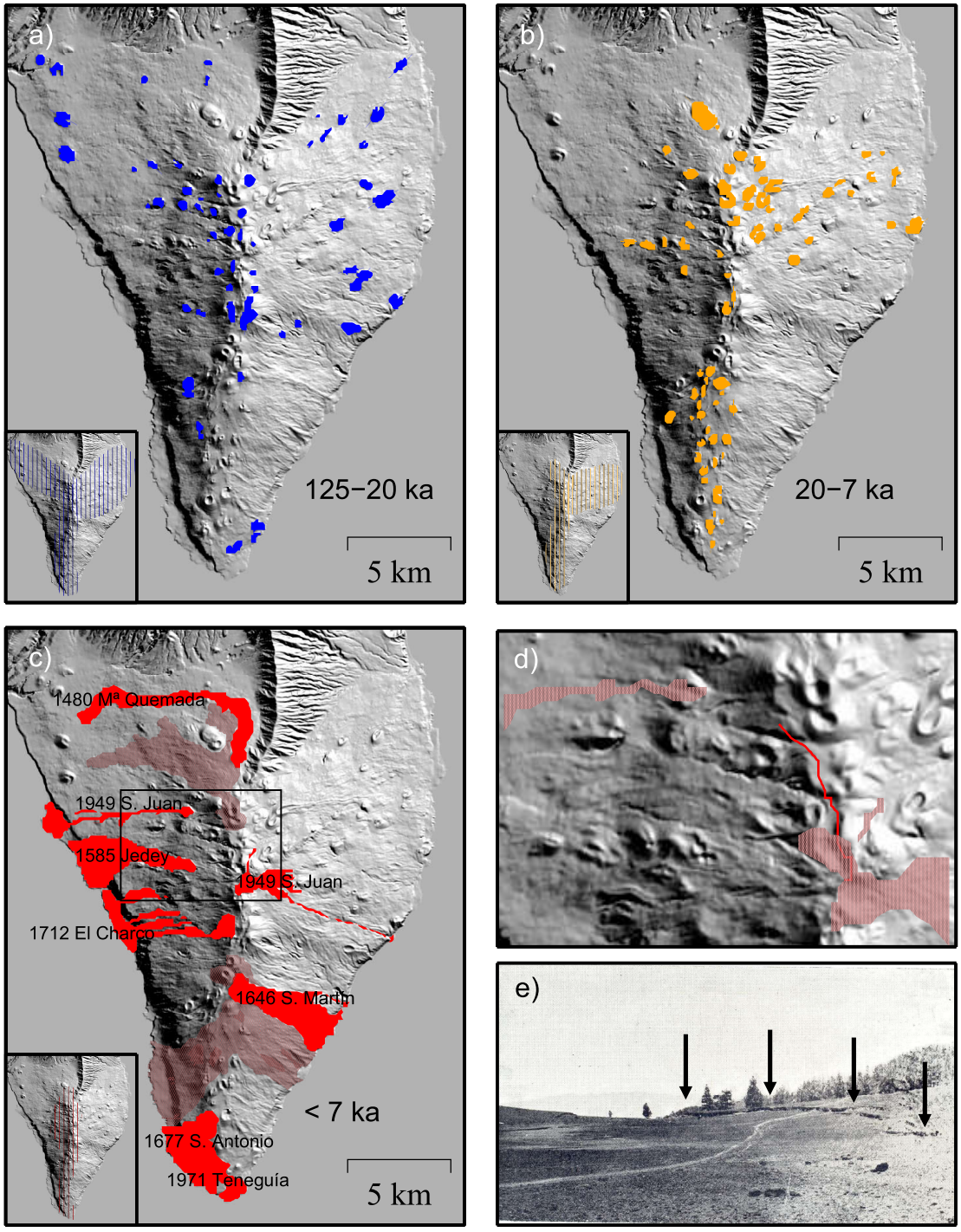
a)
125–20 ka
5 km
b)
20–7 ka
5 km
c)
1480 Mª Quemada
1949 S. Juan
1585 Jedey
1949 S. Juan
1712 El Charco
1646 S. Martín
< 7 ka
1677 S. Antonio
1971 Teneguía
5 km
d)
e)

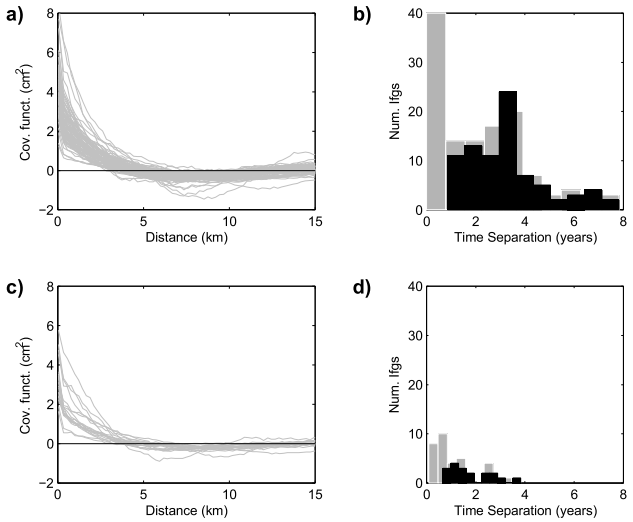
a)
b)
c)
d)
Cov. funct. (cm²)
Distance (km)
Num. Ifgs
Time Separation (years)

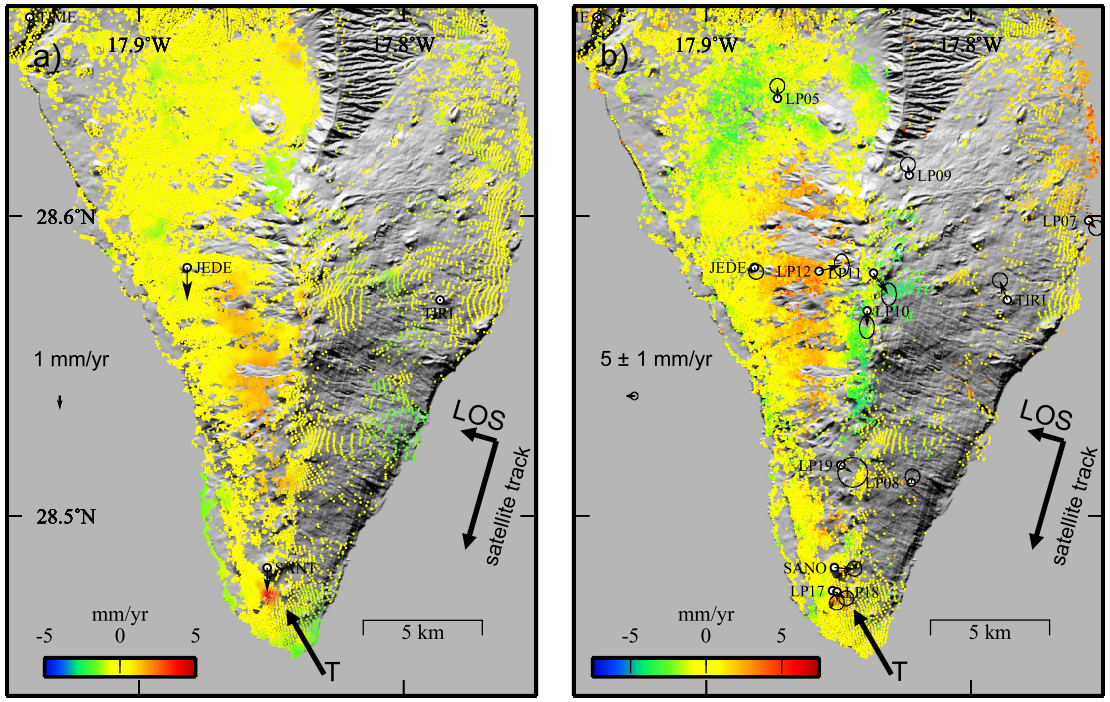
a)
17.9°W
17.8°W
28.6°N
28.5°N
JEDE
TIRI
1 mm/yr
LOS
satellite track
mm/yr
-5
0
5
5 km
T
b)
LP05
LP09
LP07
LP12
LP11
LP10
5 ± 1 mm/yr
LP19
LP08
SANO
LP17
LP18

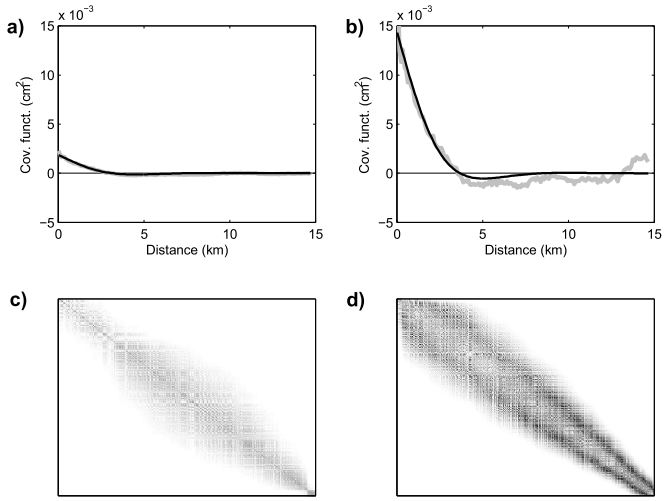
a)
b)
c)
d)
x 10^-3
Cov. funct. (cm^2)
Distance (km)
15
10
5
0
−5
0
5
10
15

to download Figure: Figure7.pdf

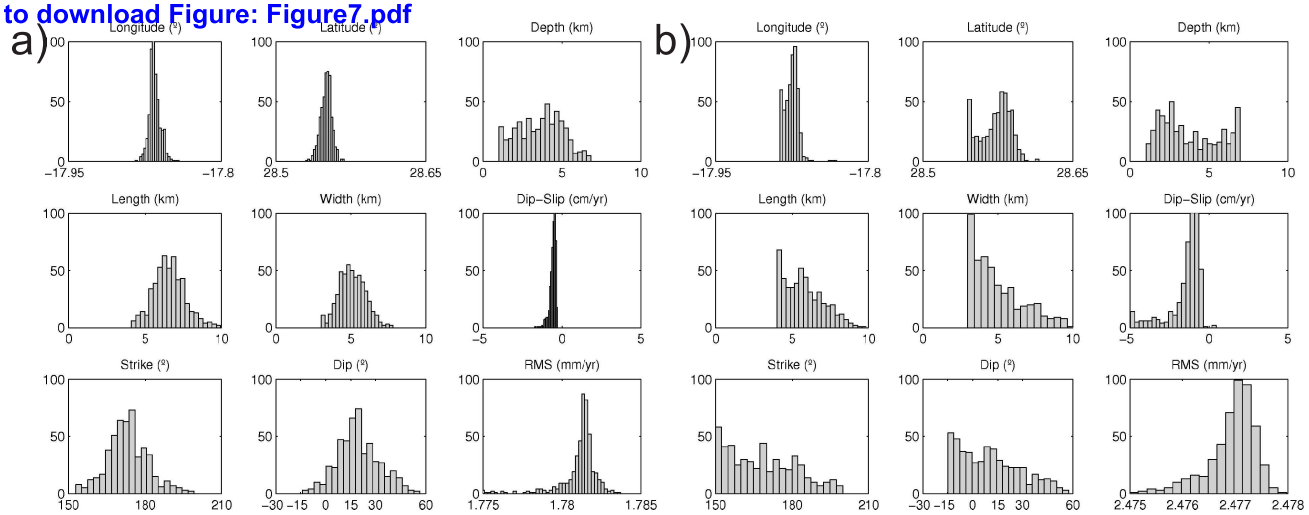

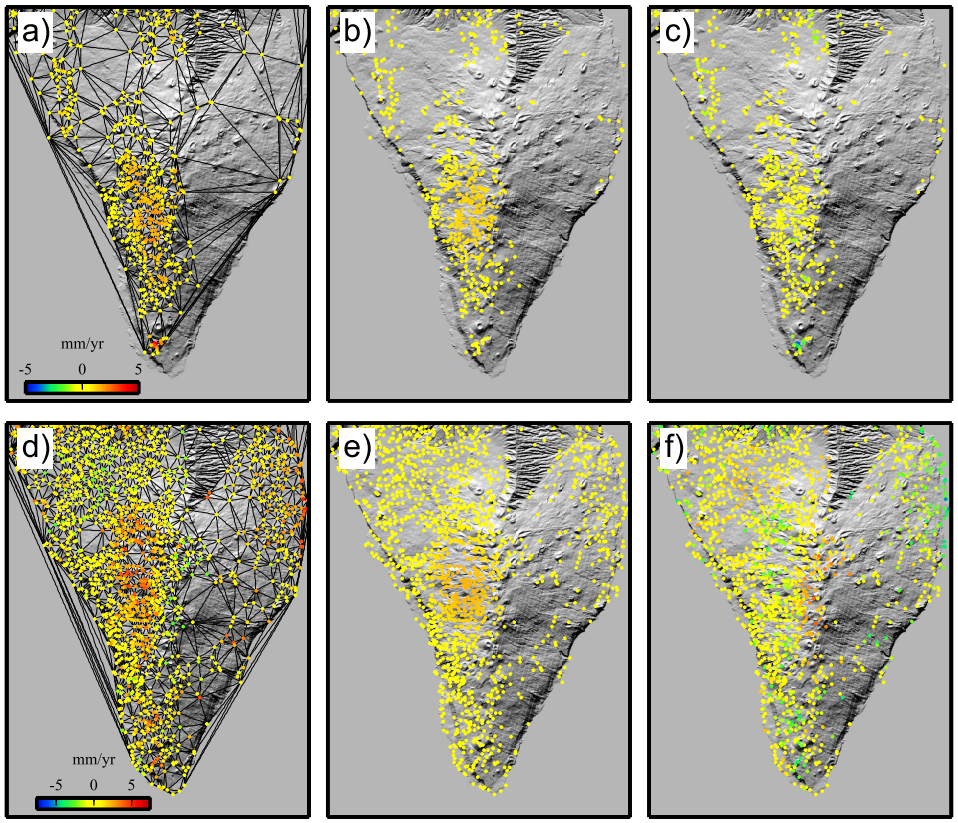
a)
b)
c)
d)
e)
f)
mm/yr
-5
0
5
mm/yr
-5
0
5

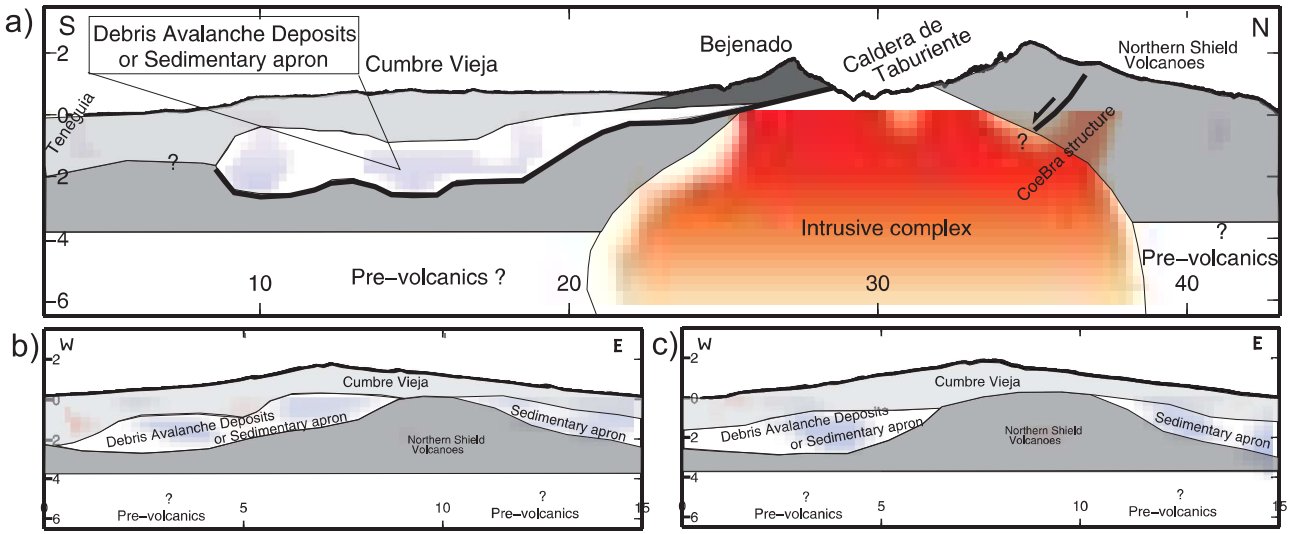
a)
S
N
Debris Avalanche Deposits
or Sedimentary apron
Cumbre Vieja
Bejenado
Caldera de
Taburiente
Northern Shield
Volcanoes
Tenguia
CoeBra structure
Intrusive complex
Pre–volcanics ?
Pre–volcanics
b)
W
E
Cumbre Vieja
Debris Avalanche Deposits
or Sedimentary apron
Sedimentary apron
Northern Shield
Volcanoes
Pre–volcanics
c)
W
E
Cumbre Vieja
Debris Avalanche Deposits
or Sedimentary apron
Sedimentary apron
Northern Shield
Volcanoes
Pre–volcanics

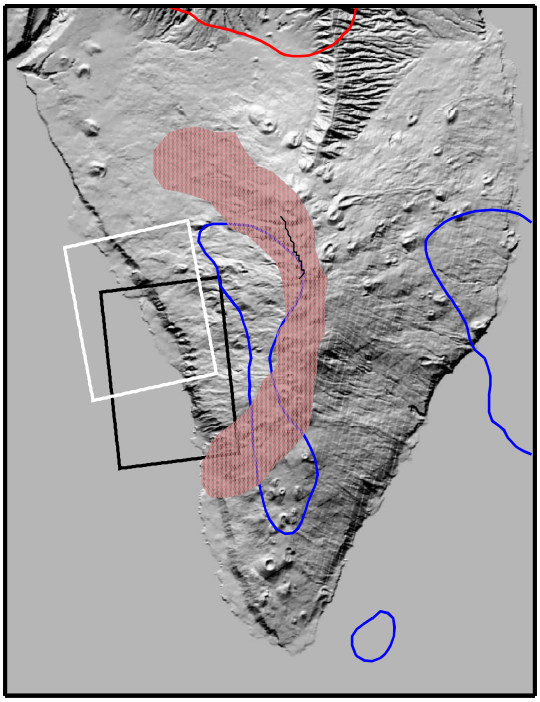

Supplementary material for on-line publication only

Click here to download Supplementary material for on-line publication only: SupplMaterial_Gonzalezetal_revised.doc